Supporting Information

A Lead-Free Zero-Dimensional Mn–Sb Hybrid Halide Enabling Blue-Light-Driven Near-Infrared Emission and X-ray Imaging

Shaobo He [a], Tao Huang [a], Ou Xu [b], Wenjie Huang [c], Quan Zhao [a], Yongqiang Zhao [a], Jiaren Huang [a], Xuda Kan [a], Bingsuo Zou[a]*

[a] Guangxi Key Lab of Processing for Nonferrous Metals and Featured Materials and Key Lab of New Processing Technology for Nonferrous Metals and Materials, Ministry of Education, School of Resources, Environments and Materials, Guangxi University, Nanning 530004, China

[b] School of Materials Science and Engineering, Huazhong University of Science and Technology, Wuhan 430074, China

[c] School of Physical Sciences and Engineering Technology, Guangxi University, Nanning 530004, China

***Corresponding Authors**

E-mail addresses:

zoubs@gxu.edu.cn. (Prof. **B. Zou**)

Full postal addresses:

School of Resources, Environment and Materials, Guangxi University, 100 Daxue East Road, Nanning, Guangxi, 530004, P.R. China.

Experimental Sections

Materials

Manganese(II) bromide tetrahydrate ($MnBr_2 \cdot 4H_2O$, 98%), antimony(III) bromide ($SbBr_3$, 99%), methyltriphenylphosphonium bromide ($C_{19}H_{20}BrP$), and ethanol (EtOH, 99.5%) were purchased from Aladdin Reagent Co., Ltd. All chemicals were used as received without further purification.

Synthesis of $[C_{19}H_{18}P]_2MnBr_4$ and Sb^{3+}-Doped $[C_{19}H_{18}P]_2MnBr_4$ Crystals

$MnBr_2 \cdot 4H_2O$ (1 mmol) and $C_{19}H_{20}BrP$ (2 mmol) were dissolved in 10 mL of ethanol and sonicated until complete dissolution was achieved. The precursor solution was then exposed to air and left undisturbed for 6 h. As the solvent gradually evaporated, block-shaped crystals of $[C_{19}H_{18}P]_2MnBr_4$ were obtained. Sb^{3+}-doped $[C_{19}H_{18}P]_2MnBr_4$ crystals were synthesized under identical conditions, except that an additional x mmol of $SbBr_3$ was introduced into the precursor solution.

Preparation of NIR-LED:

A phosphor-converted NIR-LED was fabricated by using a commercial 450 nm blue LED chip as the excitation source and $[C_{19}H_{18}P]_2MnBr_4$:6%Sb powder as the NIR-emitting conversion layer. Specifically, the as-prepared $[C_{19}H_{18}P]_2MnBr_4$:6%Sb phosphor powder was uniformly mixed with transparent AB glue to form a homogeneous slurry. The resulting mixture was then coated onto the surface of a commercial 450 nm LED chip. Before measurements, the coated device was treated in a vacuum environment at 60 °C for 60 min to ensure good adhesion and uniformity of the phosphor layer. The electroluminescence (EL) spectra of the as-fabricated NIR-LED were recorded under different driving currents to evaluate its output performance.

Preparation of 6% Sb^{3+}-Doped $[C_{19}H_{18}P]_2MnBr_4$/PDMS Composite Film

The $[C_{19}H_{18}P]_2MnBr_4$:6%Sb^{3+} powder was uniformly mixed with PDMS, followed by vacuum treatment at 50 °C for 12 h to obtain the 6% Sb^{3+}-doped $[C_{19}H_{18}P]_2MnBr_4$/PDMS composite film.

Characterization

Powder X-ray diffraction (XRD) patterns were collected on a Rigaku D/MAX 2500V

18 kW diffractometer using Cu Kα radiation (λ = 1.54059 Å) over a 2θ range of 5°–60°. Morphological observations were carried out using scanning electron microscopy (SEM, Zeiss Sigma 500). The simulated PXRD pattern was generated from the reported CIF crystallographic data of the $P2_1$ phase using the VESTA program and was used for qualitative comparison with the experimental PXRD data. Elemental composition and distribution were analyzed by energy-dispersive spectroscopy (EDS, Oxford X-max20). Raman spectra were recorded using a WITec alpha300R Raman spectrometer with a 633 nm laser as the excitation source. Photoluminescence (PL), photoluminescence excitation (PLE), time-resolved photoluminescence (TRPL, 2048 channels), temperature-dependent PL spectra, and photoluminescence quantum yield (PLQY) measurements were performed on an FLS-1000 spectrometer (Edinburgh Instruments) equipped with a PLQY accessory. UV–vis absorption spectra were recorded using a Shimadzu UV-3600PLUS spectrophotometer. The electroluminescence (EL) spectra of the as-fabricated NIR-LED were recorded using a HOPOO HPCS6500 system under different driving currents to evaluate its output performance. For NIR imaging demonstrations, the fabricated NIR-LED was employed as the illumination source, and the transmitted/reflected NIR signal from the target object was recorded using an NIR camera to generate grayscale images. Radioluminescence (RL) spectra were recorded by an Edinburgh FS5 instrument excited by a MOXTEK MAGPRO TUB00154-9I-06 70 kV X-ray tube. During the testing process, the X-ray tube was placed in a sealed lead box to avoid the harm of X-rays to the human body. The light yield was estimated by using a LuAG:Ce wafer with the same size as the referential scintillator. The relationship between RL intensity and X-ray dose rate was obtained by adjusting the dose-rate range, and the detection limit in dose rate was derived from the slope of the fitting line with a signal-to-noise ratio of 3. For X-ray imaging, the as-prepared $(C_{19}H_{18}P)_2MnBr_4$:6%Sb phosphor was embedded into a PDMS matrix to fabricate a flexible scintillation screen, which was directly used for imaging tests in a homemade X-ray imaging system. The X-ray tube was operated at 40 kV and 40 μA, and the X-ray images were recorded using a B&W CMOS FL 20BW camera. The spatial resolution of the scintillation screen was evaluated by

comparison with a standard line-pair card.

Computational Details

All density functional theory (DFT) calculations were carried out using the Vienna Ab initio Simulation Package (VASP).[1] The exchange–correlation functional was described within the generalized gradient approximation (GGA) using the Perdew–Burke–Ernzerhof (PBE) parameterization, together with the projector-augmented wave (PAW) method.[2] Ultra-soft pseudopotentials were employed for all elements. The plane-wave kinetic energy cutoff was set to 520 eV, and a 2 × 2 × 4 Monkhorst–Pack k-point mesh was used for Brillouin zone sampling. The energy convergence criterion for structural relaxation was set to 1.0×10^{-5} eV.

Element	4%	6%	8%	10%
Br (%)	80.24	79.21	79.64	79.41
Mn (%)	19.21	20.09	19.35	18.02
Sb (%)	0.35	0.51	0.65	0.71

Table S1. Comparison of element concentrations obtained from EDS analysis of *x*%Sb^{3+}-doped $[C_{19}H_{18}P]_2MnBr_4$.

Bond	Undoped (Å)	Sb-doped (Å)	Δ (Å)
Mn–Br1	2.4387	2.4491	+0.0104
Mn–Br2	2.4302	2.4211	−0.0091
Mn–Br3	2.4288	2.4396	+0.0108
Mn–Br4	2.4630	2.4619	−0.0011
Average Mn–Br	2.4402	2.4429	+0.0027

Table S2. DFT-optimized local Mn–Br bond lengths of undoped and Sb-doped $(C_{19}H_{18}P)_2MnBr_4$

Bond angle	Undoped (°)	Sb-doped (°)	Δ (°)
Br1–Mn–Br2	113.7884	112.4306	−1.3578
Br1–Mn–Br3	108.2388	108.7642	+0.5254
Br1–Mn–Br4	107.8408	107.7299	−0.1109
Br2–Mn–Br3	110.7844	109.3422	−1.4422
Br2–Mn–Br4	103.7887	107.3023	+3.5136
Br3–Mn–Br4	112.3122	111.2216	−1.0906

Table S3. DFT-optimized local Br–Mn–Br bond angles of undoped and Sb-doped $(C_{19}H_{18}P)_2MnBr_4$

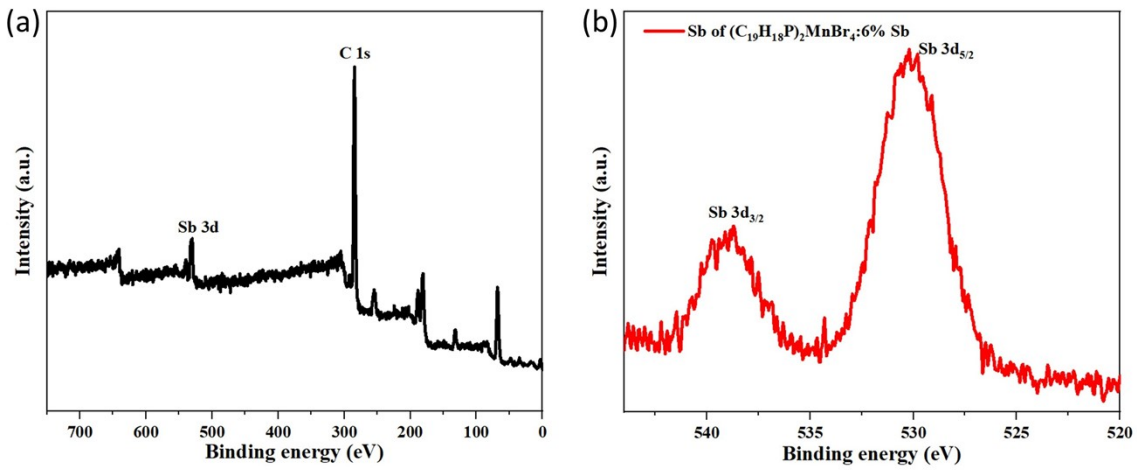

Figure S1. XPS spectra of $(C_{19}H_{18}P)_2MnBr_4$:6%Sb: (a) survey spectrum and (b) high-resolution Sb 3d spectrum.

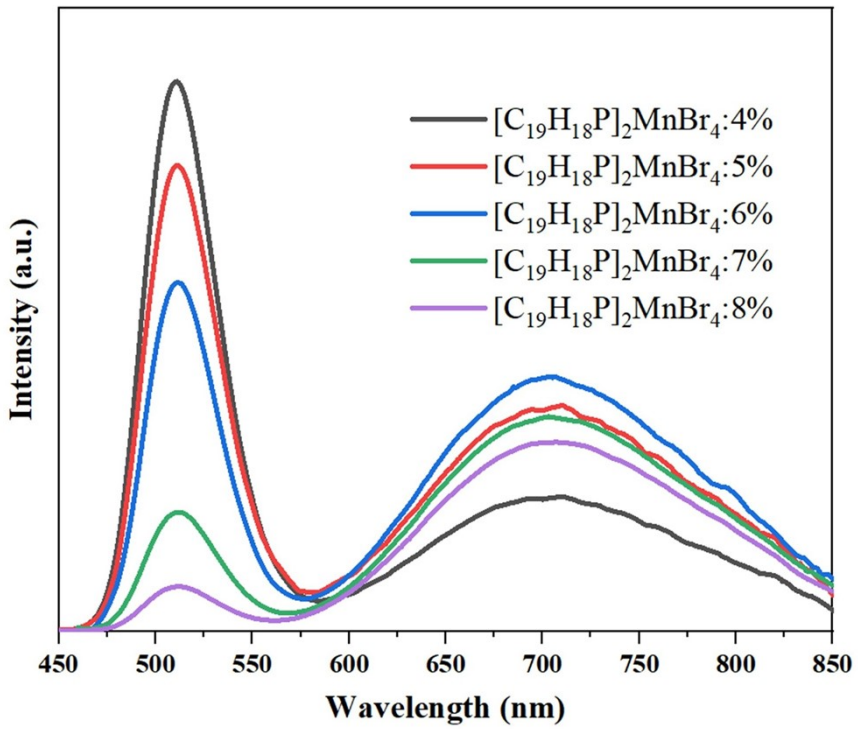

Figure S2. PL spectra of $[C_{19}H_{18}P]_2MnBr_4$:x%Sb.

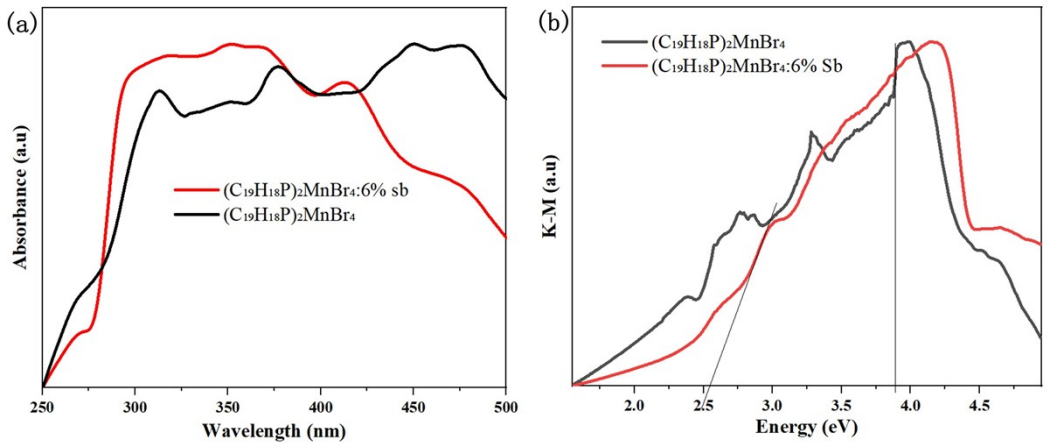

Figure S3. (a) Optical absorption spectra, and (b) band gaps of $[C_{19}H_{18}P]_2MnBr_4$ and $[C_{19}H_{18}P]_2MnBr_4$:6%Sb.

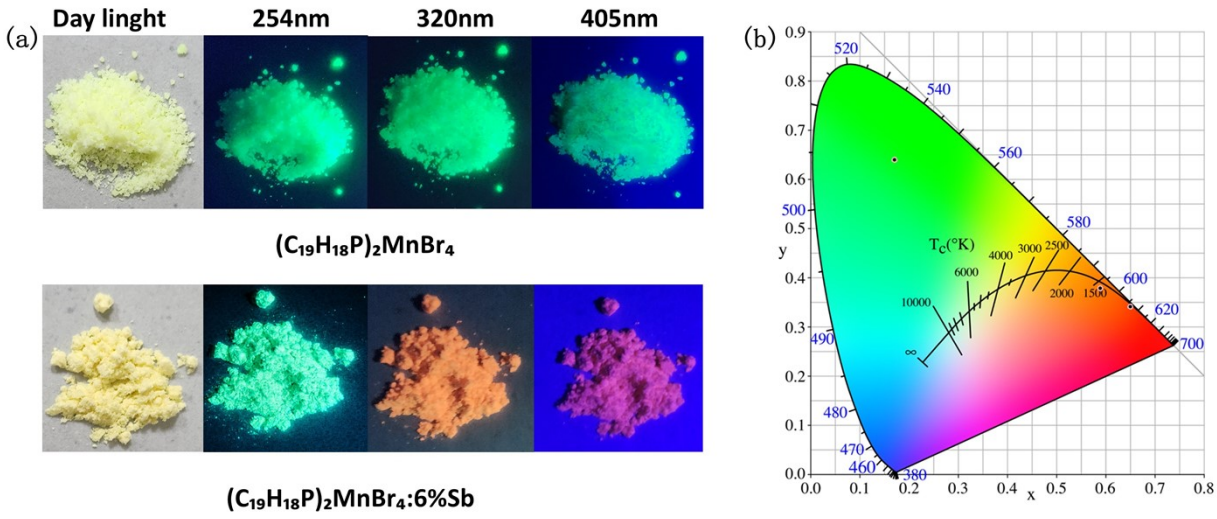

Figure S4. (a) Optical photographs of $[C_{19}H_{18}P]_2MnBr_4$ and $[C_{19}H_{18}P]_2MnBr_4$:6%Sb under different excitation wavelengths. (b) Corresponding CIE chromaticity diagram showing the color coordinates of the emission.

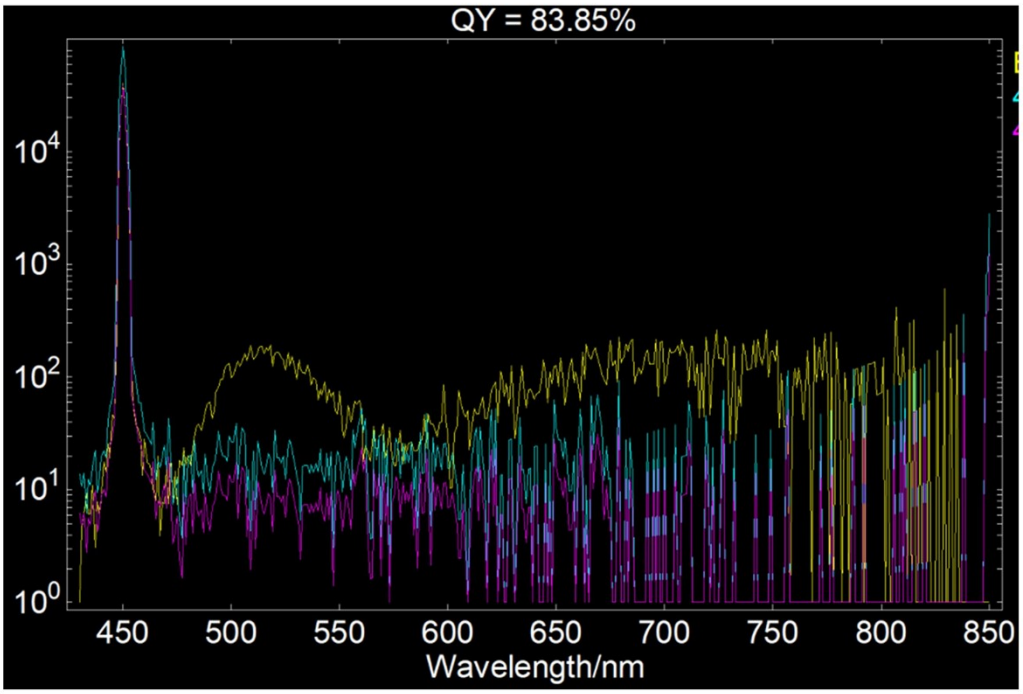

Figure S5. The PLQY of $(C_{19}H_{18}P)_2MnBr_4$:6%Sb under 450 nm excitation.

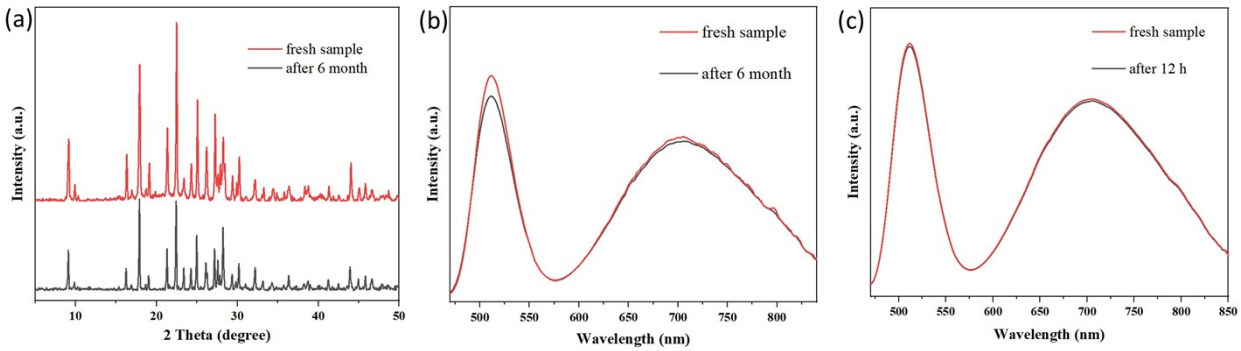

Figure S6. (a) PXRD patterns of fresh $(C_{19}H_{18}P)_2MnBr_4$:6%Sb and the sample stored in ambient air (25 °C, 55% RH) for 6 months. (b) PL spectra of fresh $(C_{19}H_{18}P)_2MnBr_4$:6%Sb and the sample stored in ambient air (25 °C, 55% RH) for 6 months. (c) PL spectra of fresh $(C_{19}H_{18}P)_2MnBr_4$:6%Sb and the sample after 12 h of continuous illumination.

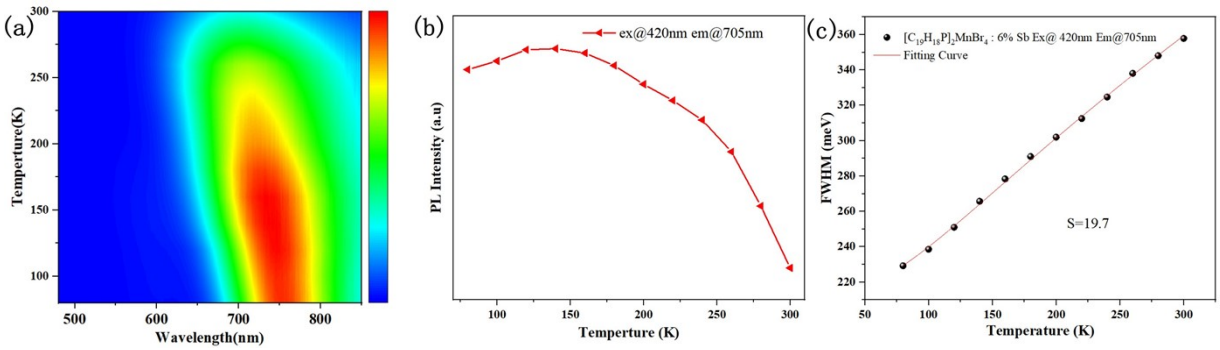

Figure S7. (a) Temperature-dependent PL spectra of $[C_{19}H_{18}P]_2MnBr_4$:6%Sb under 420 nm excitation, (b) the evolution of the PL peak intensity at 705 nm, and (c) the corresponding Huang–Rhys factor derived for the 705 nm emission band.

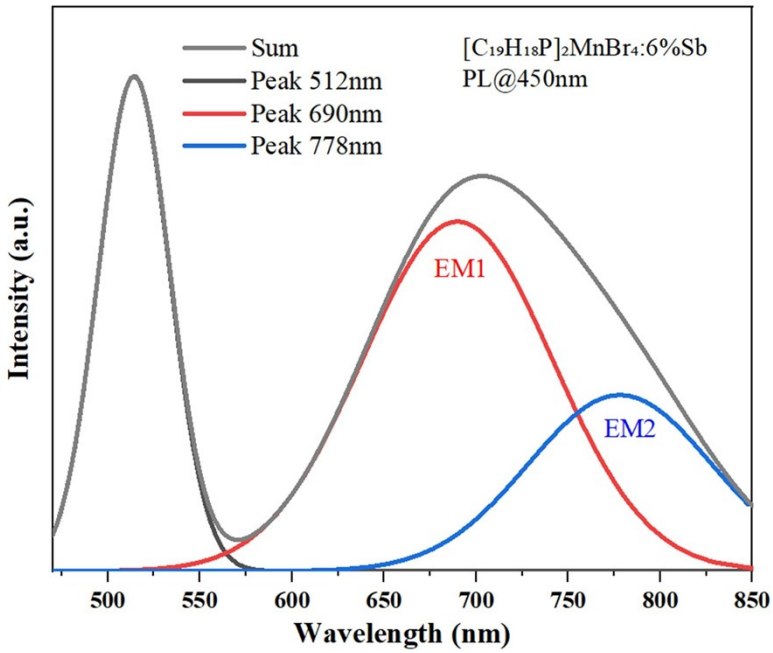

Figure S8. Peak deconvolution of the PL spectrum of $(C_{19}H_{18}P)_2MnBr_4$:6%Sb under 450 nm excitation, showing two long-wavelength components centered at approximately 690 nm (EM1) and 778 nm (EM2).

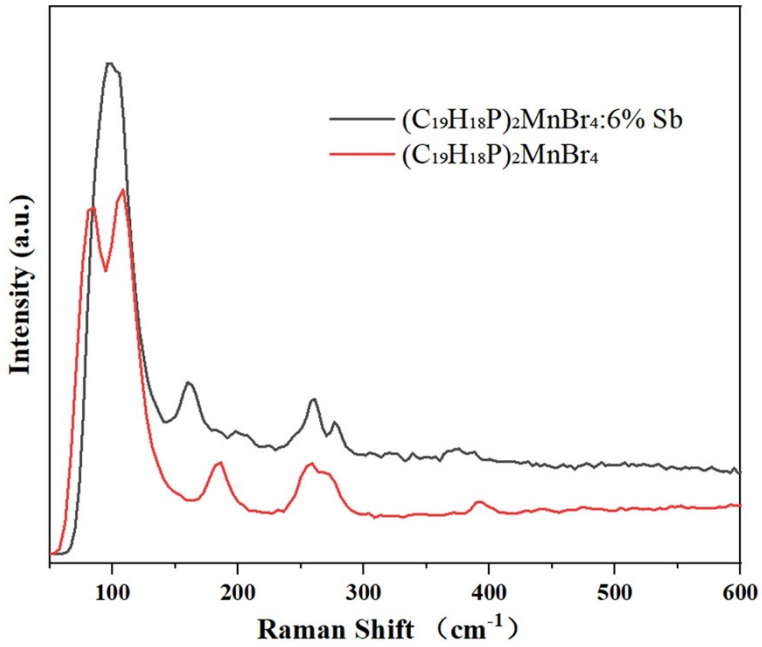

Figure S9. The Raman spectra of $[C_{19}H_{18}P]_2MnBr_4$ and $[C_{19}H_{18}P]_2MnBr_4$:6%Sb

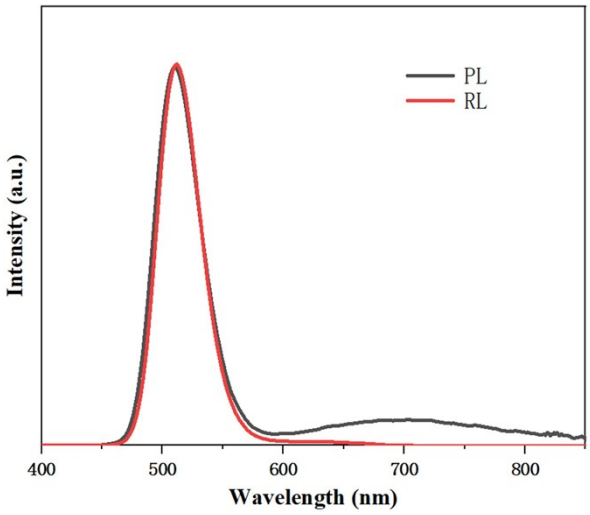

Figure S10. The normalized PL and RL spectra of $[C_{19}H_{18}P]_2MnBr_4$:6%Sb

References:

1 P. E. Blöchl, *Phys. Rev. B*, 1994, **50**, 17953.

2 G. Kresse and J. Furthmüller, *Phys. Rev. B*, 1996, **54**, 11169.